Supplementary Information

Experimental section

Materials: Sodium Tungstate Dihydrate ($Na_2WO_4 \cdot 2H_2O$), Copper chloride hexahydrate ($CuCl_2 \cdot 6H_2O$), Anhydrous sodium sulfate (Na_2SO_4), Sodium nitrite ($NaNO_2$), acetone (C_3H_6O), anhydrous ethanol (C_2H_6O), ammonium chloride (NH_4Cl), sodium hydroxide (NaOH), salicylic acid ($C_7H_6O_3$), sodium citrate dihydrate ($C_6H_5Na_3O_7 \cdot 2H_2O$), p–dimethylamino benzaldehyde ($C_9H_{11}NO$), and sodium nitroferricyanide dihydrate ($C_5FeN_6Na_2O \cdot 2H_2O$) were purchased from Chengdu Kelong Ltd.

Preparation of $CuWO_4$: Typically, 1mmol of $Na_2WO_4 \cdot 2H_2O$ and 1mmol of $CuCl_2 \cdot 6H_2O$ were dissolved in 30 mL of deionized water, and stirred for one hour. Finally, the solution was transferred to a 50 ml sealed Teflon-lined stainless steel autoclave. Then the autoclave was kept at 180 °C for 16 h. After the autoclave cooled down to room temperature, the catalysts were taken out and washed with water and ethanol several times, and subsequently dried at 60 ºC overnight. The catalyst was then calcined in air at 500 °C for 2 h. Finally, the catalyst $CuWO_4$ was obtained.

Preparation of CuO: Typically, dissolve 5 mmol of copper nitrate and 30 mmol of urea in 40 mL of deionized water, stirring for one hour. The solution is then transferred into a 100 mL sealed stainless steel autoclave lined with polytetrafluoroethylene. The autoclave is subsequently maintained at 90°C for 14 h. After cooling to room temperature, the catalyst is removed, washed multiple times with water and ethanol, and dried overnight at 60°C. It is then calcined at 300°C for 2 h in air, yielding the final

CuO catalyst.

Preparation of WO_3: A solution of Na_2WO_4 (0.33 g dissolved in 20 mL of water) was placed under stirring. Then, 20 mL of a 0.1 M HCl solution was slowly added dropwise under vigorous stirring. The solution is then transferred into a 100 mL sealed stainless steel autoclave lined with polytetrafluoroethylene. and maintained at 180 °C for 16 h. After the reaction, the autoclave was allowed to cool down to room temperature naturally. The product was collected by centrifugation, washed several times with water and ethanol, and dried overnight at 60 °C. Finally, the obtained sample was calcined in air at 500 °C for 2 h to remove organic residues and enhance crystallinity, yielding WO_3 nanoparticles.

Characterizations: XRD data were acquired by an X-ray diffractometer with Cu Kα radiation (DX-2700B). SEM measurements were carried out on an X-ray diffractometer with Cu Kα radiation (DX-2700B). The absorbance data were measured on UV–vis spectrophotometer of SHIMADZU UV-2600. TEM image was obtained from an atomic-resolution scanning transmission electron microscopy (FEI Talos F200S Super) operated at 200 kV. XPS measurements were performed with Thermo Fischer ESCALAB Xi^+.

Electrochemical measurements: All electrochemical measurements were carried out in an H−shaped electrochemical cell separated by Nafion 117 membrane using a CHI 760E electrochemical workstation (Chenhua, Shanghai). The $CuWO_4$ nanoparticles loaded on carbon cloth serve as the working electrode. The area of the working electrode immersed in the electrolyte is 0.25 cm^{-2}. LSV was performed in Ar−saturated

0.5 M Na_2SO_4 with 0.1 M $NaNO_2$ at a scan rate of 5 mV s^{-1}. All potentials reported in this work were converted to a reversible hydrogen electrode (RHE) scale, and current densities were normalized to the geometric surface area. All experiments were carried out at room temperature (25 °C).

DEMS was conducted using an in-situ mass spectrometer (Linglu QAS100) combined with an electrochemical workstation. A small electrolytic cell with a volume of 2 mL was used, and the electrolyte was bubbled with high-purity Ar gas for 30 min to remove O_2 and N_2. A Pt wire and an Ag/AgCl electrode were used as the counter and reference electrodes, respectively. In situ mass spectrometry was performed simultaneously with constant potential electrolysis tests to detect products and intermediates.

H_2 determination was performed using a gas chromatograph (Shimadzu GC-2014C) and an electrochemical workstation. An H-type cell was employed, with a platinum sheet and Ag/AgCl electrode serving as the counter electrode and reference electrode, respectively. The electrolyte was purged with high-purity Ar gas to remove O_2 and N_2. GC testing was conducted concurrently with the constant-potential electrolysis experiments. The generated H_2 was quantified using a gas chromatograph equipped with a thermal conductivity detector (TCD). Ar was used as the carrier gas. During the experiment, a flow meter is used to monitor and control the carrier gas flow rate. The system is equipped with an automatic sampler to ensure stable and repeatable injection volumes. H_2 quantification is accomplished using a calibration curve established with certified standard mixed gases.

Determination of NH_3: The NH_3 concentration in the electrolyte was determined (the obtained electrolyte was diluted 20 times) by the indophenol blue method. Specifically, 2 mL of electrolyte collected after electrolysis was mixed with 2 mL of coloring solution (1 M NaOH containing 5% salicylic acid and 5% sodium citrate) and 1 mL of oxidizing solution (0.05 M NaClO). Then, 0.2 mL oxidation solution (0.05 M NaClO) mL catalyst solution (1 wt% $C_5FeN_6Na_2O$ $2H_2O$) were dropped into the collected solution. After standing in the dark for 2 h, the concentration of NH_3 was determined by UV–Vis at a specific wavelength of 655 nm. The concentration−absorbance curve was calibrated using the standard NH_4Cl solution with known concentrations of 0.0, 0.25, 0.5, 1.0, 1.5, 2.0, and 2.5 μg mL^{-1} in 0.5 M Na_2SO_4. The fitting curve (y = 0.41418x + 0.02591, R^2 = 0.9998) shows a good linear relation of absorbance value with NH_3 concentration.

Determination of FE and NH_3 yield:

The NH_3 FE is estimated from the charge consumed for NO_2^- reduction and the total charge passed through the electrode:

$$FE = 6 \times F \times V \times [NH_3] / (Q \times 17) \times 100\%$$

The yield rate of NH_3 (aq) is calculated:

$$NH_3 \text{ yield} = V \times [NH_3] / (A \times t \times 17)$$

Where $[NH_3]$ is the concentration of NH_3, F is the Faradaic constant (96485 C mol^{-1}), V is the volume of electrolyte in the anode compartment (45 mL), Q is the total charge passing the electrode, t is the electrolysis time, and A is the geometric surface area.

DFT calculation details: First-principles calculations with spin-polarized were performed based on density functional theory (DFT) implemented in the VASP package.[1] The interaction between valence electrons and ionic core was expanded using the projector augmented wave (PAW)[2] approach with cutoff of 500 eV and 450 eV for the bulk and slab models, respectively. Perdew-Burke-Ernzerhof functional (PBE) with semi-empirical corrections of DFT-D3 was adopted to describe the exchange-correlation functional effect[3] based on general gradient approximation (GGA). $CuWO_4$ (111) slab with the thickness of the vacuum region is >15 Å was built. The Hubbard U model was implemented with an effective U = 7.5 eV for Cu, while the U correction is unnecessary for the W atoms.[4] The Brillouin zone was sampled by $4 \times 4 \times 1$ special k-points using the Monkhorst Pack scheme for structural configuration optimizations.[5] The force convergence thresholds are 0.02 eV/Å and the total energy is less than 1E-5 eV, respectively.

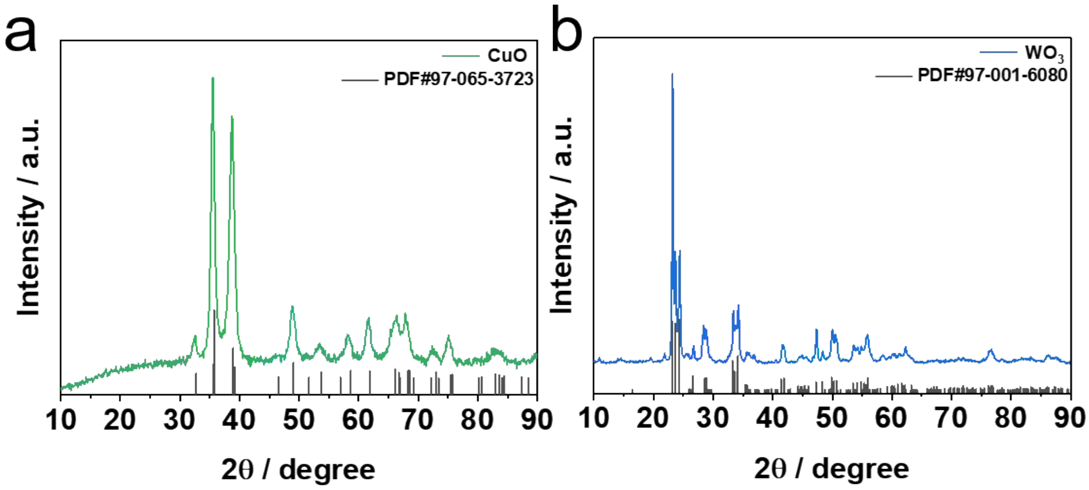

Fig. S1 XRD spectra of (a) WO_3 and (b) CuO.

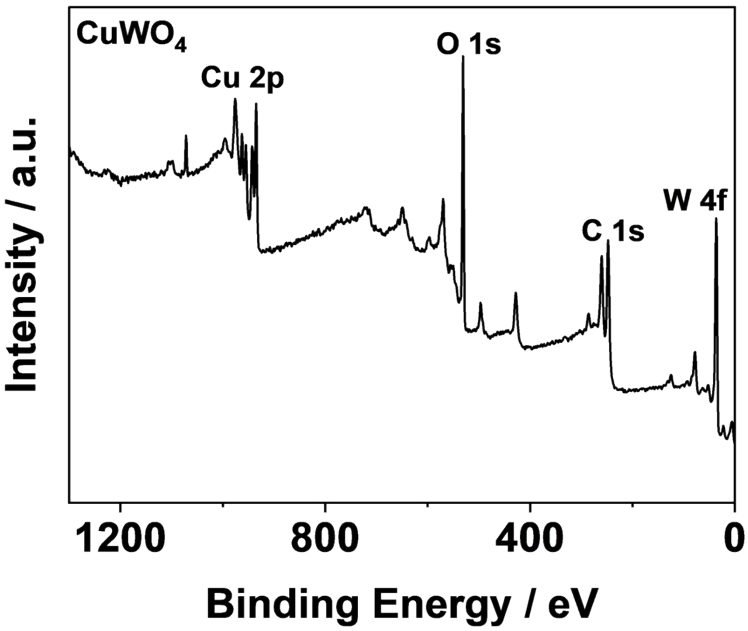

Fig. S2 XPS survey spectrum of $CuWO_4$.

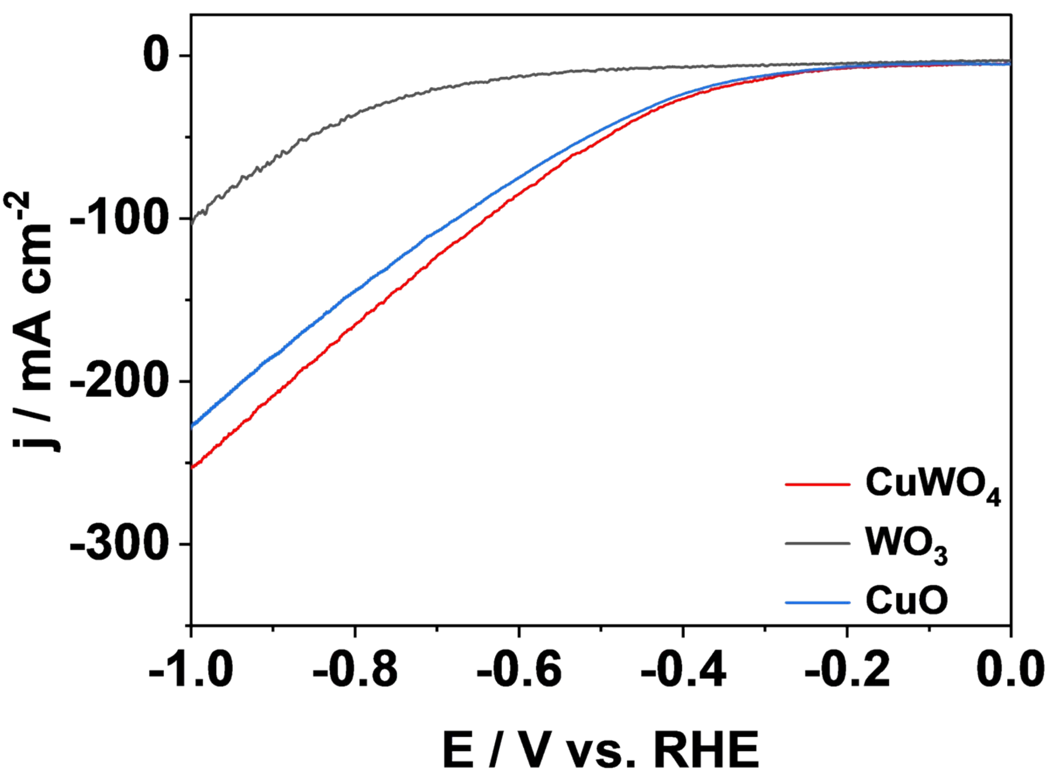

Fig. S3 LSV curves of $CuWO_4$, WO_3, and CuO tested in 0.5 M Na_2SO_4 solution with 0.1 M $NaNO_2$.

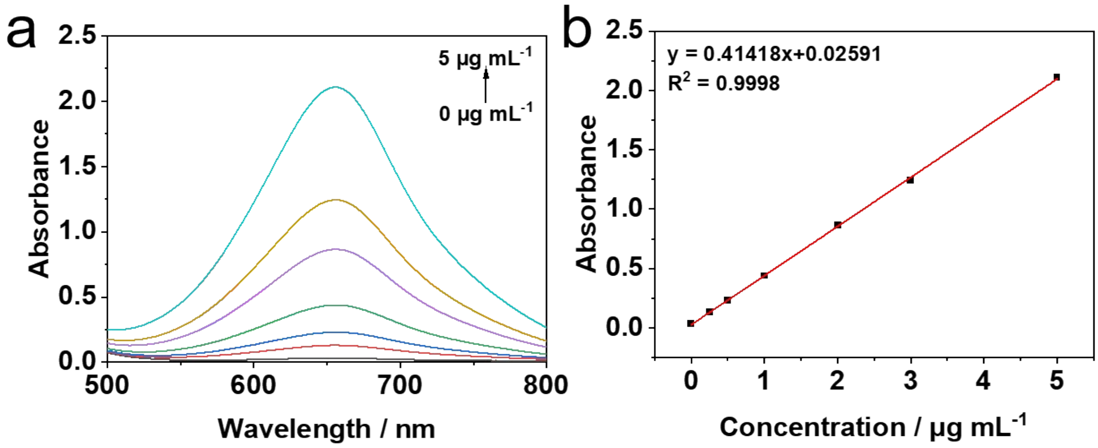

Fig. S4 (a) UV−Vis spectra and (b) corresponding calibration curves were used to calculate NH_4^+.

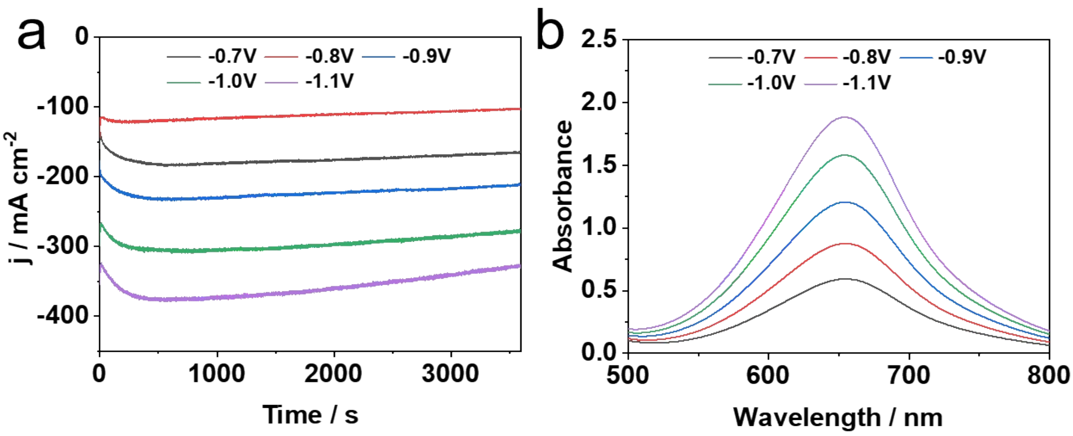

Fig. S5 (a) Chronoamperometry curves and (b) corresponding UV–Vis spectra of $CuWO_4$ from –0.7 V to –1.1 V.

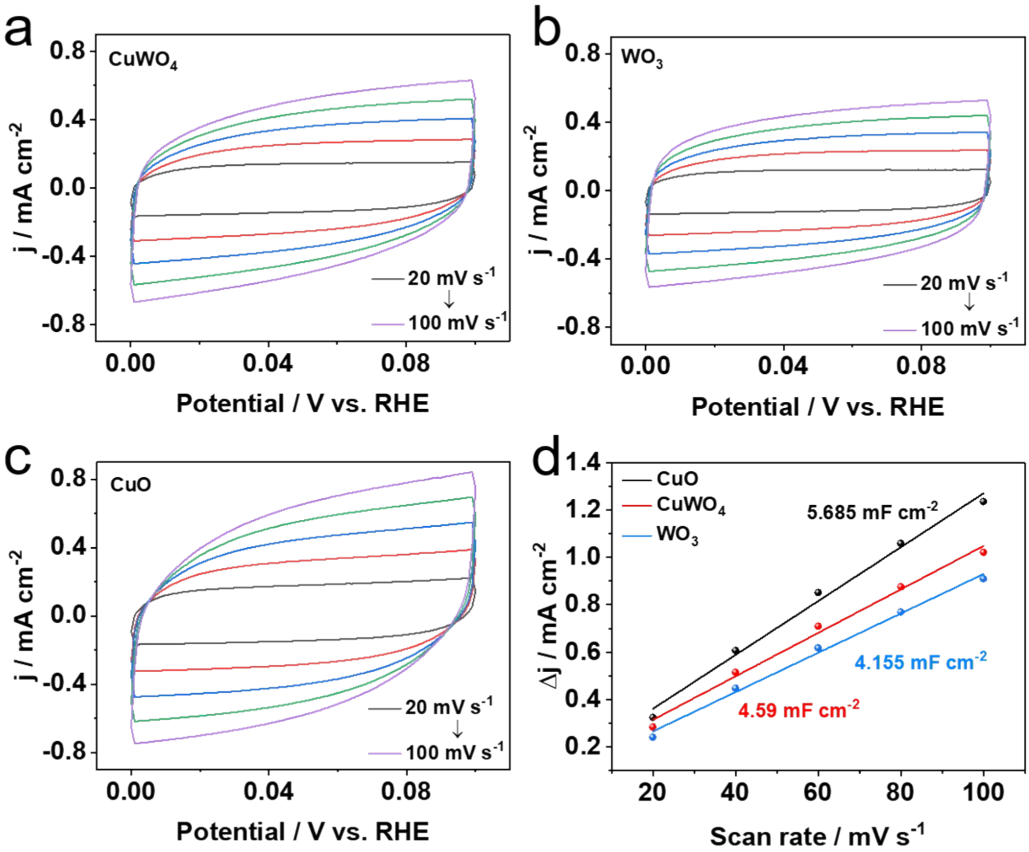

Fig. S6 CV curves of (a) $CuWO_4$, (b) WO_3, and (c) CuO at different scan rates (20–100 mV s^{-1}). (d) C_{dl} of $CuWO_4$, WO_3, and CuO.

Electrochemically active surface area (ECSA) can be estimated from double-layer capacitance (C_{dl}) using the following formula: ECSA = C_{dl} / C_s, where C_{dl} is the experimentally measured double-layer capacitance and Cs is the specific capacitance per unit true surface area, whose value depends on material properties and electrolyte type. For copper-based materials, the literature commonly employs the accepted value of C_s = 40 μF cm^{-2} (see Power Sources, Appl. Surf. Sci., 2022, 585, 152757). Thus, the electrochemical surface area calculations are as follows: ECSA ($CuWO_4$) = 4.59 / 40 × 10^{-3} cm^2 = 114.75 cm^2 ECSA (CuO) = 5.685 / 40 × 10^{-3} cm^2 = 142.125 cm^2, ECSA (WO_3) = 4.155 / 40 × 10^{-3} cm^2 = 103.875 cm^2.

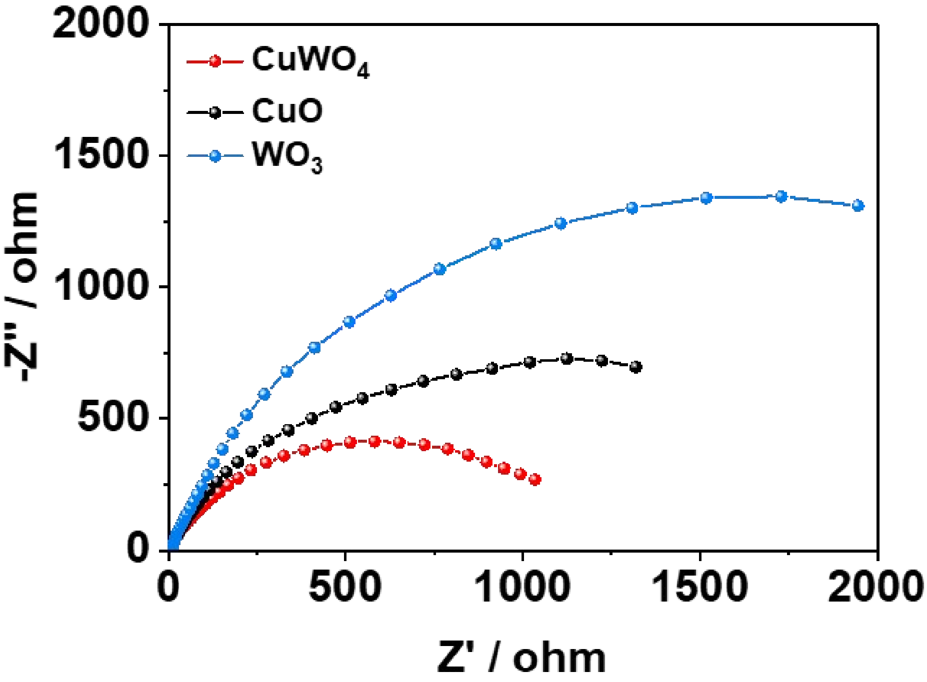

Fig. S7 Nyquist plots for $CuWO_4$, WO_3, and CuO.

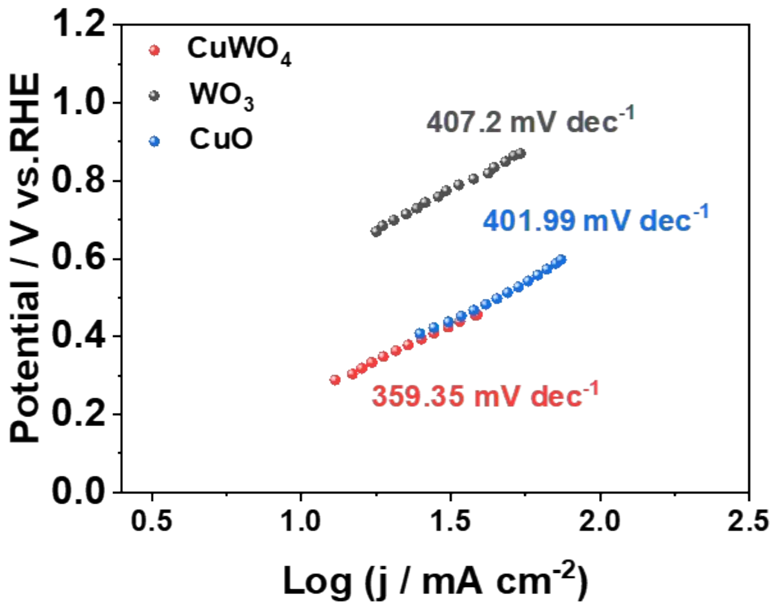

Fig. S8 Tafel slopes of $CuWO_4$, WO_3, and CuO.

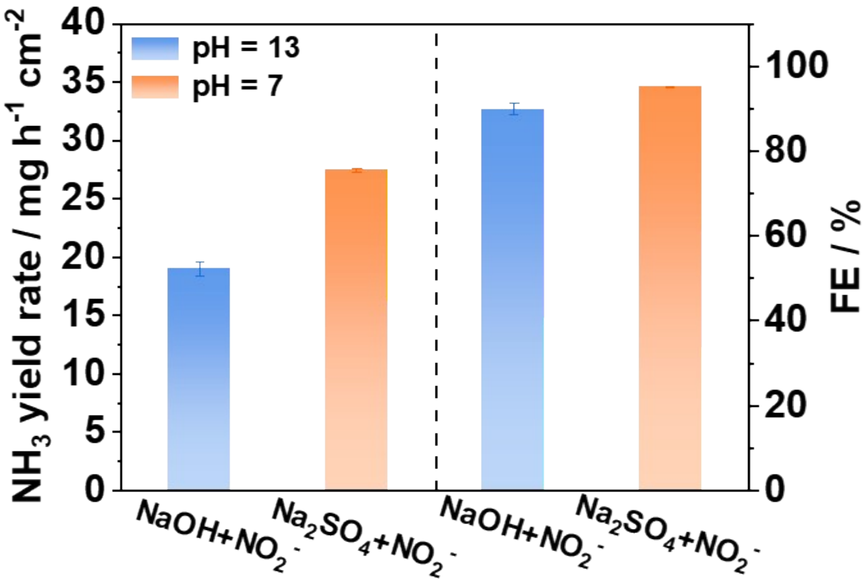

Fig. S9 NH_3 yield and FE at different pH at -1.0V.

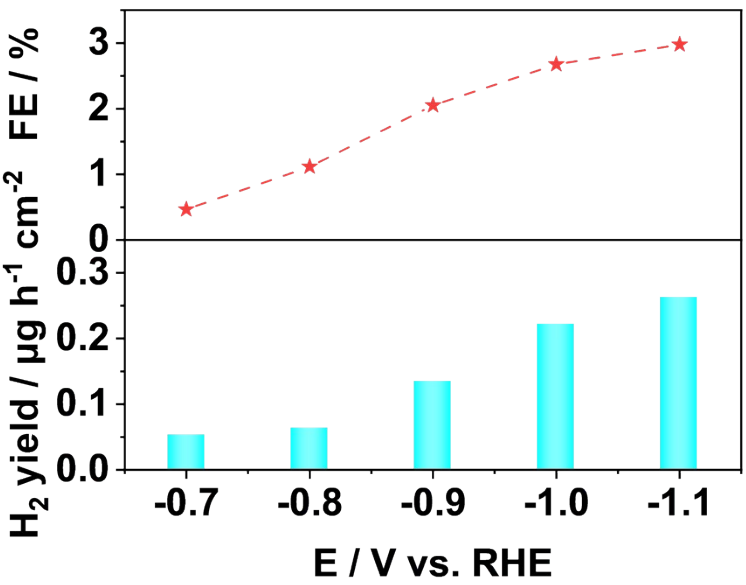

Fig. S10 H_2 yield and FE during NO_2^-RR electrolysis at various potentials.

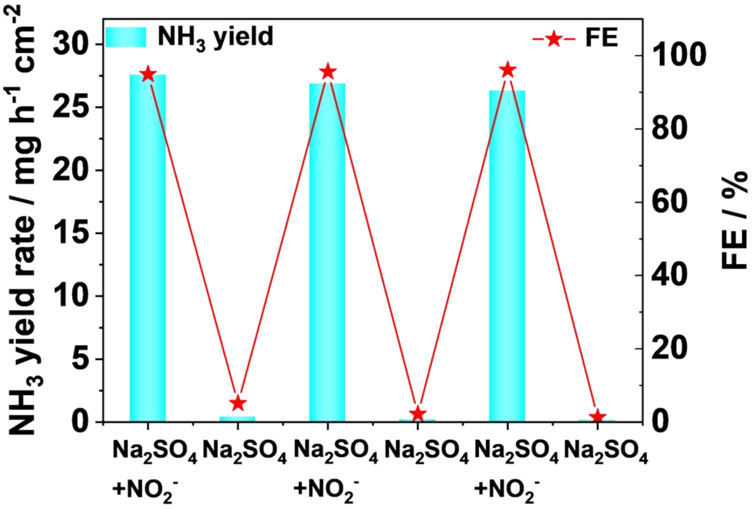

Fig. S11 NH_3 yield and FE of $CuWO_4$ were evaluated during alternating cycling tests.

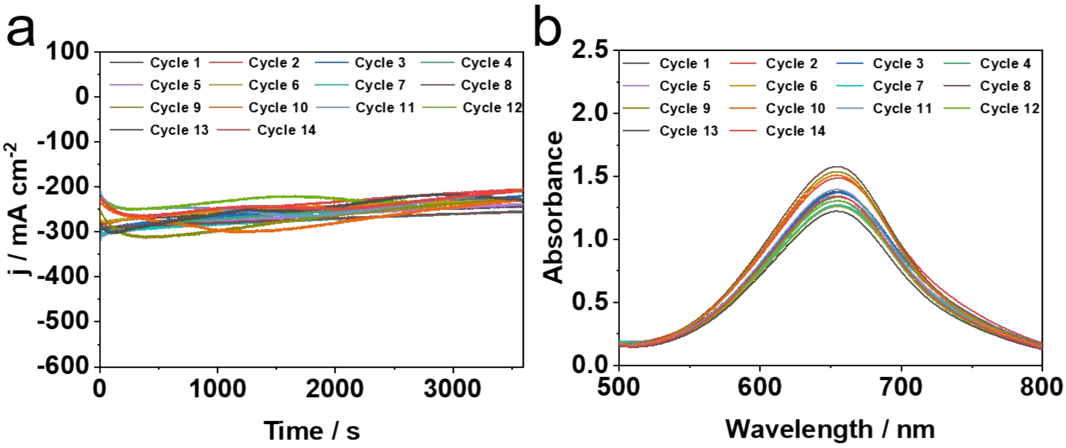

Fig. S12 (a) Chronoamperometry curves and (b) corresponding UV−Vis absorption spectra of $CuWO_4$ during cycling tests in 0.5 M Na_2SO_4 with 0.1 M NO_2^- at −1.0 V.

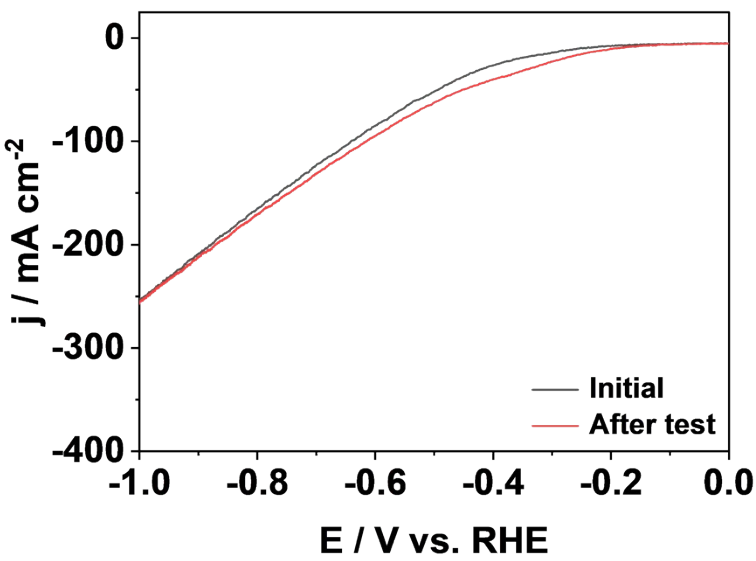

Fig. S13 LSV curves before and after the stability test.

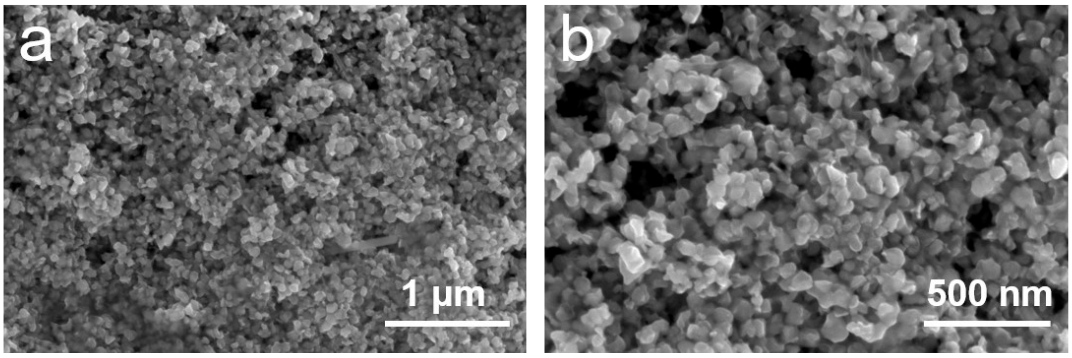

Fig. S14 SEM images of $CuWO_4$ nanoparticle after long-term electrolysis.

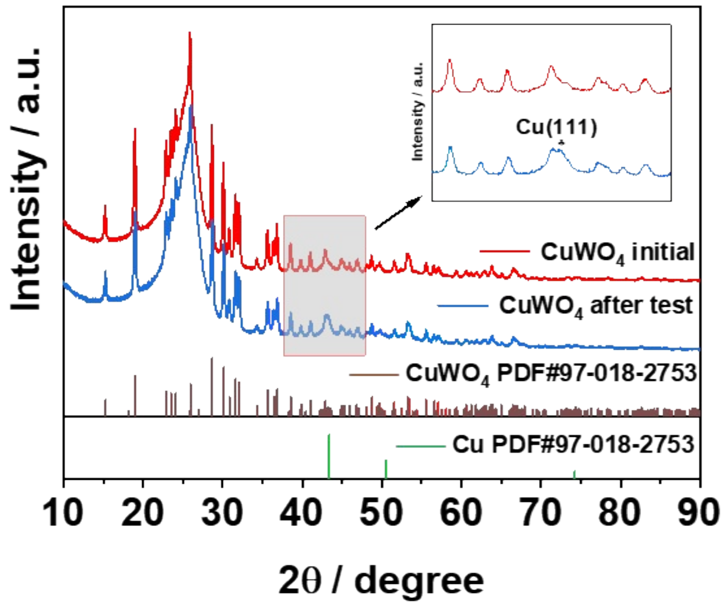

Fig. S15 XRD spectra of $CuWO_4$ nanoparticles loaded on carbon cloth before and after long-term electrolysis.

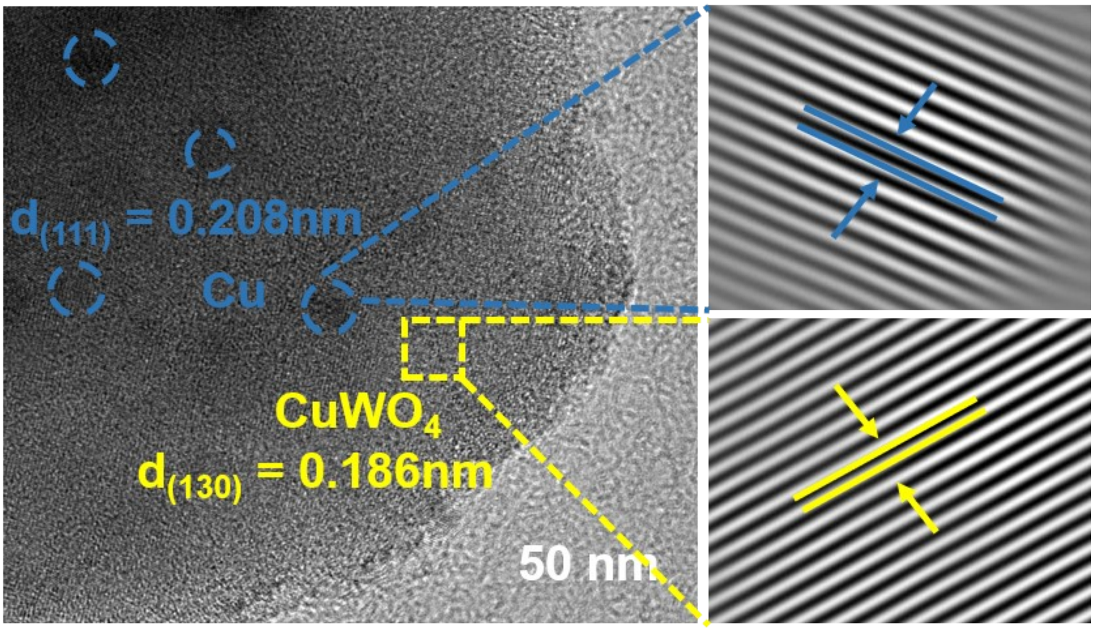

Fig. S16 HRTEM images of $CuWO_4$ nanoparticle after long-term electrolysis.

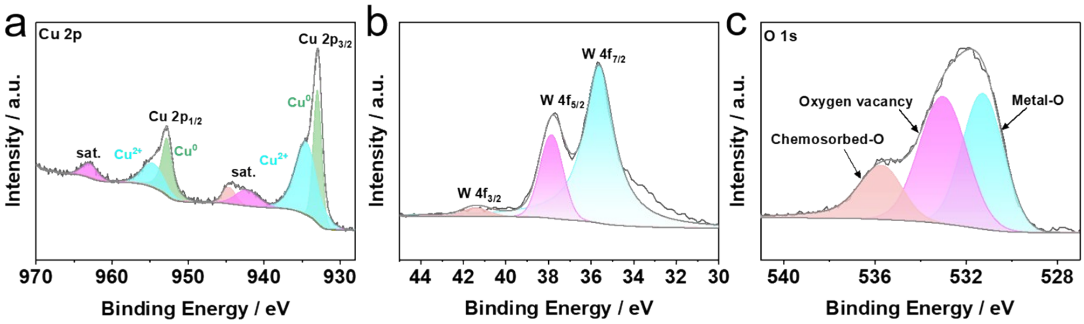

Fig. S17 High-resolution XPS spectra of (a) Cu 2p, (b) W 4f, and (c) O 1s of $CuWO_4$ nanoparticles after long-term electrolysis.

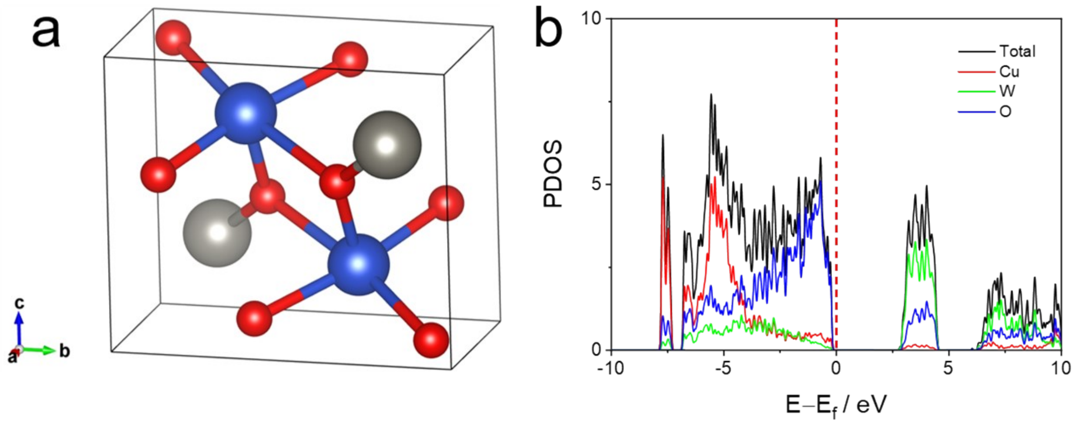

Fig. S18 (a) Atomic structure of $CuWO_4$ after lattice optimization and (b) corresponding PDOS.

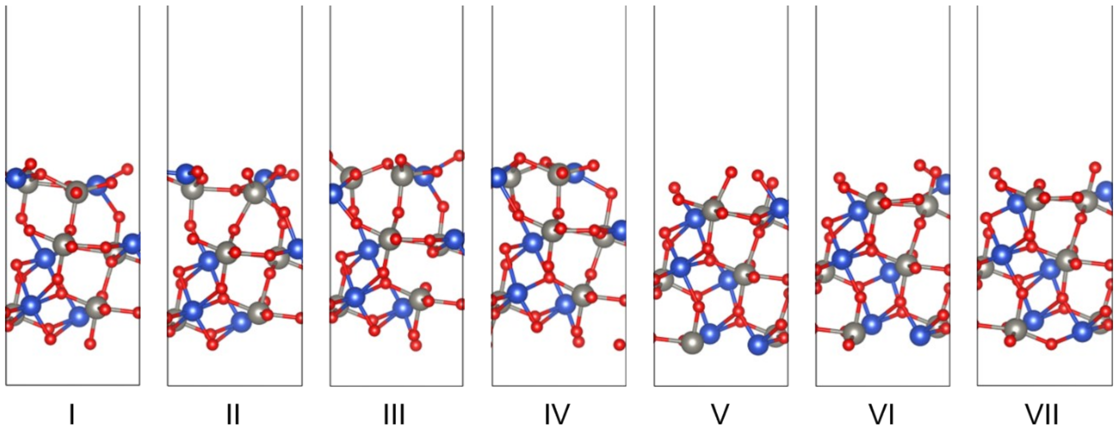

Fig. S19 Atomic structure of $CuWO_4$ (111) slab model with various terminated surfaces. Blue, grey, and red represent Cu, W, and O, respectively.

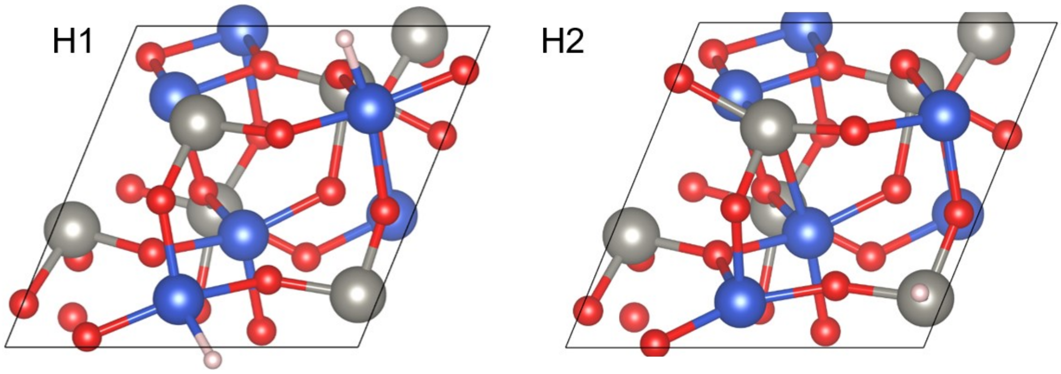

Fig. S20 Corresponding atomic structure of HER processing on different sites of $CuWO_4$ (111).

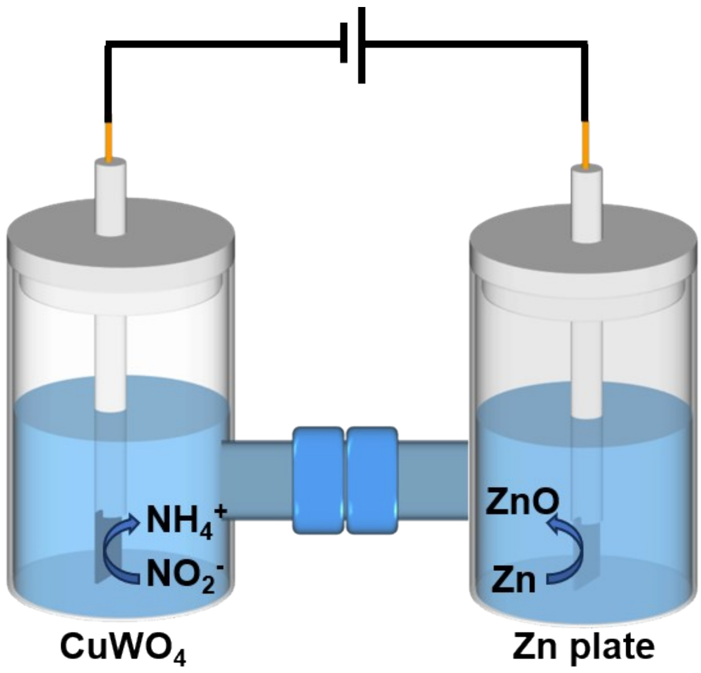

Fig. S21 Schematic diagram of a Zn-$NO_2^−$ battery.

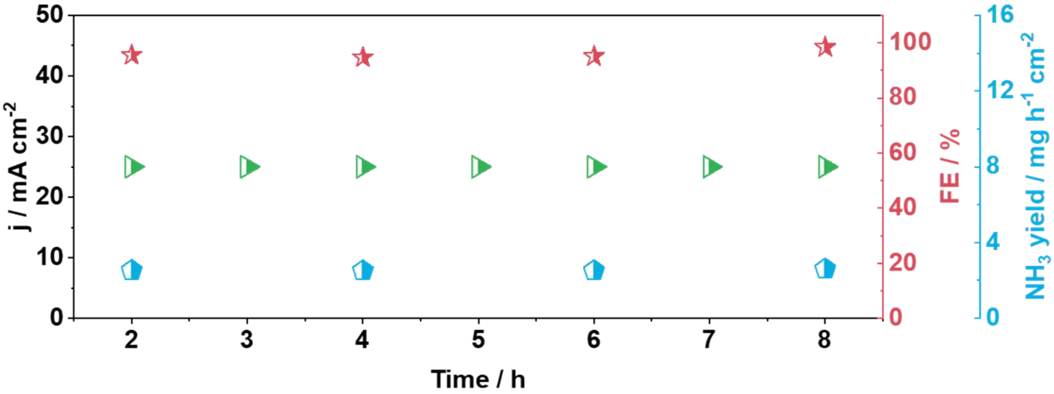

Fig. S22 Long-term NO_2^-RR experiment and the corresponding NH_3 yields and FE with the Zn-NO_2^- battery.

Table S1. Comparison of the catalytic performance of $CuWO_4$ with other reported NO_2^-RR electrocatalysts.

Catalyst	Electrolyte	Potential (V vs RHE)	FE (%)	NH_3 yield rate	Refs.
$CuWO_4$	**0.5 M Na_2SO_4 (0.1 M $NaNO_2$)**	**–1.0 V**	**95.09**	**27.46 mg h^{-1} cm^{-2}**	**This work**
$NiWO_4$/NF	0.1 M NaOH (0.1 M $NaNO_2$)	–0.4V	97.6	10.974 mg h^{-1} cm^{-2}	6
Cu_3P NA/CF	0.1 M PBS (0.1 M $NaNO_2$)	–0.5V	91.2±2.5	1.626 ± 0.036 mg h^{-1} cm^{-2}	7
Mn_1/MoO_{3-x}	0.5 M Na_2SO_4 (0.5 M $NaNO_2$)	–0.6V	92.6	9.3 mg h^{-1} cm^{-2}	8
Ni-TiO_2/TP	0.1 M NaOH (0.1 M $NaNO_2$)	–0.5V	94.89	6.476 mg h^{-1} cm^{-2}	9
Ni@HPCF/CP	0.1 M NaOH (0.1 M $NaNO_2$)	–0.8V	95.1	2.41 mg h^{-1} cm^{-2}	10
TiO_{2-x} NBA/TP	0.1 M NaOH (0.1 M $NaNO_2$)	–0.7V	92.7	7.898 mg h^{-1} cm^{-2}	11
WO_2/W	0.1 M NaOH (0.1 M $NaNO_2$)	–0.9V	94.32	14.964 mg h^{-1} cm^{-2}	12
Ru-Cu NW/CF	0.1 M PBS (500 ppm NO2–)	–0.6V	94.1	12.47 mg h^{-1} cm^{-2}	13
u–Cu/CF	0.5 M Na_2SO_4 (0.1 M $NaNO_2$)	–0.7V	94.7	8.4065 mg h^{-1} cm^{-2}	14
CF@Cu_2O	0.1 M PBS (0.1 M $NaNO_2$)	–0.6V	94.2	7.53 mg h^{-1} cm^{-2}	15
Co_3S_4/NF	0.1 M NaOH (0.1 M $NaNO_2$)	–0.3V	96.9	19.2 mg h^{-1} cm^{-2}	16
Cu/N-SnS_{2-x}	0.1 M NaOH (0.1 M $NaNO_2$)	−0.835	95.7	3.775 mg h^{-1} cm^{-2}	17

FeCu DAC	0.1 M KOH ($0.1\ M\ NaNO_2$)	−0.6V	99.88	4.905 mg h^{-1} cm^{-2}	18
TiO_2@CoFe-LDH	0.1 M NaOH ($0.1\ M\ NaNO_2$)	−0.6V	97.4	17.99 mg h^{-1} cm^{-2}	19
Sb_1Cu	$0.5\ M\ Na_2SO_4$ ($0.1\ M\ NaNO_2$)	−0.6V	96.4	10.41 mg h^{-1} cm^{-2}	20
FeOOH NTA/CC	0.1 M PBS ($0.1\ M\ NaNO_2$)	−1.0V	94.7	11.96 mg h^{-1} cm^{-2}	21
$CoWO_4$/NF	$0.5\ M\ Na_2SO_4$ ($0.1\ M\ NaNO_2$)	−0.7V	95.2	18.856 mg h^{-1} cm^{-2}	22
NiCo–TiO_2	0.1 M NaOH ($0.1\ M\ NaNO_2$)	−0.4V	97.5	18.736 mg h^{-1} cm^{-2}	23

Table S2. Comparison of NH_3 yield and power density of our battery with recent Zn-N_2, Zn-NO, Zn-NO_2^-, or Zn-NO_3^- battery systems.

Catalyst	Battery Type	Power density	Refs.
$CuWO_4$	**Zn-NO_2^-**	**7.63**	**This work**
Cu NDs	Zn-N_2	0.01	24
Fe-2HCS-8	Zn-N_2	0.15	25
NbS_2	Zn-N_2	0.31	26
CoPi/NPCS	Zn-N_2	0.49	27
Ti_2O_3	Zn-N_2	1.02	28
Nb_2O_5/Nb_2CTX	Zn-N_2	1.25	29
$FePS_3$	Zn-N_2	2.60	30
TiO_{2-x}/TP	Zn-NO	0.84	31
MoS_2/CP	Zn-NO	1.04	32
a-$B_{2.6}C@TiO_2/Ti$	Zn-NO	1.7	33
O-Fe-N_6-Cu	Zn-NO	2.30	34
CoB/Co@C	Zn-NO	3.68	35
hcp-Co	Zn-NO	4.6	36
FeOCl-V_{Cl}	Zn-NO	6.2	37
ITO@TiO_2/TP	Zn-NO_2^-	1.22	38
MoO_2	Zn-NO_2^-	2.94	39
$NiMoO_4$	Zn-NO_2^-	3.6	40
WO_{2-x}	Zn-NO_2^-	5.05	12
$NiWO_4$	Zn-NO_2^-	5.55	6
Ni-Mo-P/TiO_2	Zn-NO_2^-	6.0	41

Pd/TiO_2	$Zn-NO_3^-$	0.87	42
RhCuM-tpp	$Zn-NO_3^-$	1.54	43
RuFe/NF	$Zn-NO_3^-$	1.9	10
Fe/Ni_2P	$Zn-NO_3^-$	3.25	44
$NiCo_2O_4/CC$	$Zn-NO_3^-$	3.94	45
PdCuAg MTs	$Zn-NO_3^-$	4.8	46
$IrSAC-Co_3O_4$	$Zn-NO_3^-$	5.6	47

References

1. G. Kresse and J. Hafner, *Phys. Rev. B*, 1994, **49**, 14251–14269.
2. G. Kresse and D. Joubert, *Phys. Rev. B*, 1999, **59**, 1758–1775.
3. J. P. Perdew, K. Burke and M. Ernzerhof, *Phys. Rev. Lett.*, 1996, **77**, 3865-3868.
4. X. Chu, D. Santos-Carballal and N. H. de Leeuw, *Phys. Chem. Chem. Phys.*, 2024, **26**, 28628–28642.
5. H. J. Monkhorst and J. D. Pack, *Phys. Rev. B*, 1976, **13**, 5188–5192.
6. H. Qiu, Q. Chen, J. Zhang, X. An, Q. Liu, L. Xie, W. Yao, X. Sun and Q. Kong, *Inorg. Chem. Front.*, 2023, **10**, 3909–3915.
7. J. Liang, B. Deng, Q. Liu, G. Wen, Q. Liu, T. Li, Y. Luo, A. A. Alshehri, K. A. Alzahrani, D. Ma and X. Sun, *Green Chem.*, 2021, **23**, 5487–5493.
8. Z. Zhang, Y. Wan, S. Shang, Z. Li and K. Chu, *Fuel*, 2025, **381**, 133394.
9. Z. Cai, C. Ma, D. Zhao, X. Fan, R. Li, L. Zhang, J. Li, X. He, Y. Luo, D. Zheng, Y. Wang, B. Ying, S. Sun, J. Xu, Q. Lu and X. Sun, *Mater. Today Energy*, 2023, **31**, 101220.
10. Y. Wang, M. Sun, J. Zhou, Y. Xiong, Q. Zhang, C. Ye, X. Wang, P. Lu, T. Feng, F. Hao, F. Liu, J. Wang, Y. Ma, J. Yin, S. Chu, L. Gu, B. Huang and Z. Fan, *Proc. Nat. Acad. Sci.*, 2023, **120**, e2306461120.
11. D. Zhao, J. Liang, J. Li, L. Zhang, K. Dong, L. Yue, Y. Luo, Y. Ren, Q. Liu, M. S. Hamdy, Q. Li, Q. Kong and X. Sun, *Chem. Commun.*, 2022, **58**, 3669–3672.
12. H. Qiu, Q. Chen, X. An, Q. Liu, L. Xie, J. Zhang, W. Yao, Y. Luo, S. Sun, Q. Kong, J. Chen and X. Sun, *J. Mater. Chem. A*, 2022, **10**, 24969–24974.

13. N. Q. Tran, L. T. Duy, D. C. Truong, B. T. Nguyen Le, B. T. Phan, Y. Cho, X. Liu and H. Lee, *Chem. Commun.*, 2022, **58**, 5257–5260.
14. R. Zhang, S. Shang, F. Wang and K. Chu, *Dalton Trans.*, 2024, **53**, 3470–3475.
15. Q. Chen, X. An, Q. Liu, X. Wu, L. Xie, J. Zhang, W. Yao, M. S. Hamdy, Q. Kong and X. Sun, *Chem. Commun.*, 2022, **58**, 517–520.
16. C. Zhang, X. Wang, J. Jiang, J. Zhang, A. Liu and L. Ai, *Appl. Catal. B: Environ.*, 2025, **365**, 124991.
17. H. Li, Y. Wang, K. Wei, M. He, M. Yan, F. Peng and F. Gao, *Adv. Sci.*, 2025, **12**, 2417773.
18. Z. Bi, J. Hu, M. Xu, H. Zhang, Y. Zhou and G. Hu, *Angew. Chem. Int. Ed.*, 2024, **63**, e202313434.
19. Y. Liang, X. Fan, X. He, D. Zheng, S. Sun, Y. Luo, H. Chen and X. Sun, *Nano Res.*, 2025, **18**, 94907344.
20. F. Wang, S. Shang, Z. Sun, X. Yang and K. Chu, *ACS Nano*, 2024, **18**, 13141–13149.
21. Q. Liu, Q. Liu, L. Xie, L. Yue, T. Li, Y. Luo, N. Li, B. Tang, L. Yu and X. Sun, *Chem. Commun.*, 2022, **58**, 5160–5163.
22. B. Zhao, Q. Chen, J. Zhang, X. An, Q. Liu, L. Xie, X. Li, W. Yao and Q. Kong, *Inorg. Chem. Front.*, 2025, **12**, 1662–1668.
23. Z. Ren, B. Zhao, Q. Chen, L. Xie, J. Zhang, X. An, Q. Liu, X. Li, W. Yao and Q. Kong, *Chem. Commun.*, 2025, **61**, 5003–5006.
24. C. Du, Y. Gao, J. Wang and W. Chen, *Chem. Commun.*, 2019, **55**, 12801-12804.

25. H. Qiao, Y. Han, L. Yao, X. Xu, J. Ma, B. Wen, J. Hu and H. Huang, *Chem. Eng. J.*, 2023, **464**, 142628.

26. H. Wang, J. Si, T. Zhang, Y. Li, B. Yang, Z. Li, J. Chen, Z. Wen, C. Yuan, L. Lei and Y. Hou, *Appl. Catal. B: Environ.*, 2020, **270**, 118892.

27. J.-T. Ren, L. Chen, Y. Liu and Z.-Y. Yuan, *J. Mater. Chem. A*, 2021, **9**, 11370–11380.

28. N. Xu, Q. Cheng, M. Wang, Y. He, H. Ji and F. Rosei, *Inorg. Chem. Front.*, 2023, **10**, 7010–7017.

29. X. Dai, W. Zhang, Y. Sun, Z. Du, Z. Tao, J. Wang, W. Fang, X. Xing, Y. Chen, H. Li, H. Zheng, J. Qiu and T. Ma, *J. Energy Chem.*, 2025, **103**, 448–457.

30. H. Wang, Z. Li, Y. Li, B. Yang, J. Chen, L. Lei, S. Wang and Y. Hou, *Nano Energy*, 2021, **81**, 105613.

31. Z. Li, Q. Zhou, J. Liang, L. Zhang, X. Fan, D. Zhao, Z. Cai, J. Li, D. Zheng, X. He, Y. Luo, Y. Wang, B. Ying, H. Yan, S. Sun, J. Zhang, A. A. Alshehri, F. Gong, Y. Zheng and X. Sun, *Small*, 2023, **19**, 2300291.

32. L. Zhang, J. Liang, Y. Wang, T. Mou, Y. Lin, L. Yue, T. Li, Q. Liu, Y. Luo, N. Li, B. Tang, Y. Liu, S. Gao, A. A. Alshehri, X. Guo, D. Ma and X. Sun, *Angew. Chem. Int. Ed.*, 2021, **60**, 25263–25268.

33. J. Liang, P. Liu, Q. Li, T. Li, L. Yue, Y. Luo, Q. Liu, N. Li, B. Tang, A. A. Alshehri, I. Shakir, P. O. Agboola, C. Sun and X. Sun, *Angew. Chem. Int. Ed.*, 2022, **61**, e202202087.

34. D. Wang, X. Zhu, X. Tu, X. Zhang, C. Chen, X. Wei, Y. Li and S. Wang, *Adv.*

Mater., 2023, **35**, 2304646.

35. B. Wu, L. Huang, L. Yan, H. Gang, Y. Cao, D. Wei, H. Wang, Z. Guo and W. Zhang, *Nano Lett.*, 2023, **23**, 7120–7128.
36. D. Wang, Z.-W. Chen, K. Gu, C. Chen, Y. Liu, X. Wei, C. V. Singh and S. Wang, *J. Am. Chem. Soc.*, 2023, **145**, 6899–6904.
37. X. Guo, P. Wang, T. Wu, Z. Wang, J. Li, K. Liu, J. Fu, M. Liu, J. Wu, Z. Lin, L. Chai, Z. Bian, H. Li and M. Liu, *Angew. Chem. Int. Ed.*, 2024, **63**, e202318792.
38. S. Li, J. Liang, P. Wei, Q. Liu, L. Xie, Y. Luo and X. Sun, *eScience*, 2022, **2**, 382–388.
39. G. Wang, Q. Chen, X. An, Q. Liu, L. Xie, J. Zhang, W. Yao, X. Liu, S. Sun, X. Sun and Q. Kong, *Colloid. Surf. A*, 2023, **657**, 130549.
40. G. Wang, Q. Chen, J. Zhang, X. An, Q. Liu, L. Xie, W. Yao, X. Sun and Q. Kong, *J. Colloid Interf. Sci.*, 2023, **647**, 73–80.
41. Z. Ren, Q. Chen, J. Zhang, X. An, Q. Liu, L. Xie, W. Yao, X. Sun and Q. Kong, *Mater. Today Phy.*, 2023, **36**, 101162.
42. Y. Guo, R. Zhang, S. Zhang, Y. Zhao, Q. Yang, Z. Huang, B. Dong and C. Zhi, *Energy Environ. Sci.*, 2021, **14**, 3938–3944.
43. J. Zhou, Y. Xiong, M. Sun, Z. Xu, Y. Wang, P. Lu, F. Liu, F. Hao, T. Feng, Y. Ma, J. Yin, C. Ye, B. Chen, S. Xi, Y. Zhu, B. Huang and Z. Fan, *Proc. Nat. Acad. Sci.*, 2023, **120**, e2311149120.
44. R. Zhang, Y. Guo, S. Zhang, D. Chen, Y. Zhao, Z. Huang, L. Ma, P. Li, Q. Yang, G. Liang and C. Zhi, *Adv. Energy Mater.*, 2022, **12**, 2103872.

45. Q. Liu, L. Xie, J. Liang, Y. Ren, Y. Wang, L. Zhang, L. Yue, T. Li, Y. Luo, N. Li, B. Tang, Y. Liu, S. Gao, A. A. Alshehri, I. Shakir, P. O. Agboola, Q. Kong, Q. Wang, D. Ma and X. Sun, *Small*, 2022, **18**, 2106961.

46. L. Sun, H. Yao, Y. Wang, C. Zheng and B. Liu, *Adv. Energy Mater.*, 2023, **13**, 2303054.

47. T. Jin, J. Wang, Y. Gong, Q. Zheng, T. Wang, R. Wu, Y. Lyu and X. Liu, *Chem Catalysis*, 2023, **3**.